Journal of Cleaner Production 242 (2020) 118476

Contents lists available at ScienceDirect

Journal of Cleaner Production

journal homepage: www.elsevier.com/locate/jclepro

Simultaneous removal of Pb(II) and rifampicin from wastewater by iron nanoparticles synthesized by a tea extract

Ze Lin [a], Xiulan Weng [a], Gary Owens [b], Zuliang Chen [a, *]

[a] School of Environmental Science and Engineering, Fujian Normal University, Fuzhou, 350007, Fujian Province, China
[b] Environmental Contaminants Group, Future Industries Institute, University of South Australia, Mawson Lakes Campus, Adelaide, South Australia, 5095, Australia

ARTICLE INFO

Article history:
Received 5 April 2019
Received in revised form
30 August 2019
Accepted 17 September 2019
Available online 18 September 2019

Handling editor; Cecilia Maria Villas Bôas de Almeida

Keywords:
Environmental pollution
Fe NPs
Green synthesis
Removal mechanism
Water treatment

ABSTRACT

Most environmental contaminants exist as a complex mixture of both metallic and organic pollutants and it is thus often a major challenge to remove both components simultaneously. In this paper, due to its low cost and environmentally friendliness, iron nanoparticles (Fe NPs) were successfully prepared using a one-step green synthesis for the simultaneous in-situ remediation of mixed contaminants. Specifically Fe NPs were used for the simultaneous removal of Pb(II) and rifampicin. The removal efficiency for Pb(II) and rifampicin were 100% and 91.6%, respectively. To better understand the mechanism of mixed contaminant removal by Fe NPs various characterization methods and the major conditions impacting removal efficiency were examined. It was concluded that (1) polyphenols and caffeine, both ubiquitous in green tea extracts, acted as both reducing and capping agents during the preparation of Fe NPs, reducing the agglomeration of Fe NPs and increasing their stability and reactivity; (2) the removal mechanism of contaminants involved Pb(II) being adsorbed onto the surface of Fe NPs due to the innate strong adsorption of metal ions onto iron oxides, while rifampicin and Pb(II) both interacted positively with the functional groups on the surface of Fe NPs. Overall, this study demonstrated that green synthesis Fe NPs had potential for use as inexpensive and efficient adsorbent for the simultaneous removal of both Pb(II) and rifampicin from wastewater.

1. Introduction

Rifampicin is a broad-spectrum antibiotic that has antibacterial activity against a variety of pathogenic microorganisms and is thus widely used agriculturally. However, the overuse of antibiotics in animal husbandry has seriously damaged the ecological environment (Peiris et al., 2017). Of similar concern is lead (Pb) which is a highly toxic non-biodegradability and environmentally persistent contaminant (Li et al., 2018). In particular the dual contaminant of environments with both heavy metals and antibiotics has attracted worldwide attention because the toxicity of both contaminants can be amplified resulting in increased accumulation in food webs, leading to increased rates of anemia, cancer, headache and other diseases (Li et al., 2018; Zhao et al., 2018). Therefore, the simultaneous removal of heavy metal and antibiotic from contaminated environments has become a high priority. To date significant research already has been conducted on the efficient treatment of contaminated wastewater, using various techniques including ion-exchange (Naushad, 2014), solvent extraction (Coll et al., 2012), chemical precipitation (Yan et al., 2010), Fenton oxidation (Ioannou-Ttofa et al., 2019) and membrane processes (Gao et al., 2014), where all of these methods were effective to some degree in removing both heavy metals and antibiotics. However, most of these methods suffered from a combination of high operating and infrastructure costs as well as complex processes, which made them generally unsuitable for most developing countries. In comparison, amongst the various methods commonly used for removing mixed contaminants, adsorption is often considered an effective method because of its ease of operation, generally lower operating costs, and the wide availability of a number of different adsorbents (Hudcová et al., 2018), which have consequently seen adsorption extensively applied for the removal of both organic and inorganic contaminants from aqueous solutions.

Today one of the most widely utilized adsorbents for environmental remediation is nano-iron (Fe NPs) by virtue of its abundance of reactive surface sites and high reactivity (Calderon and Fullana,

* Corresponding author.
E-mail address: zlchen@fjnu.edu.cn (Z. Chen).

https://doi.org/10.1016/j.jclepro.2019.118476
0959-6526/

2015; Mahto et al., 2018). Numerous researches have even reported Fe NPs as "the cure" for heavy metal and antibiotic pollution, which has seen it successfully adopted for the treatment of wastewater contaminated with multiple heavy metals (Bagbi et al., 2017). Chitosan stabilized bimetallic Fe/Ni nanoparticles have successfully removed amoxicillin and Cd(II) (Weng et al., 2013). Despite the removal efficiency being promising, chemical synthesis of Fe NPs is limited by high cost and the harsh chemical reagents used. Thus, there is increasing demand for the preparation new types of Fe NPs which address these limitations and are suitable for environmental remediation. Fe NPs have been green synthesized using *Euphorbia cochinchensis* leaf extract, for the degradation of 2,4-dichlorophenol (2,4-DCP) (Guo et al., 2017). Green synthesized Fe NPs prepared using *Oolong* tea extract were also successfully applied for the degradation of malachite green (Huang et al., 2014). While some success has been reported in applying iron derived nanomaterials for single contaminant removal, research on the remediation of mixed contaminant systems involving both heavy metals and antibiotics is still limited.

The main objectives of this study were to simultaneously remove Pb(II) and rifampicin from wastewater by Fe NPs prepared using a green tea extract, and to understand the removal mechanism of both heavy metal and antibiotic from the wastewater. The key issues addressed were: (1) The mechanism of removal of Pb(II) and rifampicin; including removal conditions and kinetics, (2) the characterization of Fe NPs before and after reaction with both contaminants, and (3) the practical demonstration of the removal effectiveness of Pb(II) and rifampicin from wastewater.

2. Experimental

2.1. Materials

Sodium acetate (CH_3COONa) was purchased from Guangzhou Jinhuada Chemical Reagent Co., Ltd., lead nitrate ($Pb(NO_3)_2$) was purchased from Sinopharm Chemical Reagent Co., Ltd., ferric chloride ($FeCl_3 \cdot 6H_2O$) and anhydrous ethanol (CH_3CH_2OH) were obtained from Xiqiao Science Co., Ltd., rifampicin ($C_{43}H_{58}N_4O_{12}$) with a purity of 97% was purchased from Shanghai Aladdin Bio-Chem Technology Co., Ltd. All chemical reagents were of analytical grade and used without further purification. All solutions were prepared using deionized water and a 1M HCl solution was used for pH adjustment during the adsorption experiments.

2.2. Preparation of green tea extract(GT)

An aqueous solution (1000 mL) of green tea leaves (60 g) was heated on a water bath at 80 °C for 1 h. Subsequently, the hot mixture was filtered through a 0.45 μm disposable filter to obtain fresh green tea extract (GT) which was stored in the dark at 4 °C until use in Fe NPs synthesis.

2.3. Preparation of Fe NPs

Adsorbent Fe NPs used in this study were prepared using a one step method. Briefly, CH_3COONa (16.046 g) and $FeCl_3 \cdot 6H_2O$ (5.4 g) were dissolved in the green tea extract prepared above (100 mL) of which was then heated in a water bath at 80 °C for 3 h. The solution was cooled to room temperature and solid products obtained were filtered and washed several times with absolute ethanol and deionized water, after that, the final product was dried using a vacuum freeze dryer for 48 h to obtain Fe NPs.

2.4. Characterization

Changes in crystal phase structure of Fe NPs before and after reaction were determined by X-ray diffraction (XRD) using a D8 ADVANCE X-ray diffractometer (CuKα) (Bruker, Germany) at 40 kV and 40 mA, where samples were scanned from $2\theta = 10°-90°$.

Fourier transform infrared (FTIR) spectra of solid powders were analyzed from 400 to 4000 cm^{-1} using a Nicolet 10 infrared analyzer (Thermo Fisher, USA) using the KBr disc method by co-milling 0.1% (w/w) Fe NPs with 100 mg KBr and then pressing into a thin disc suitable for FTIR analysis.

X-ray photoelectron spectroscopy (XPS) was used to examine the distribution and speciation of elements across the NPs surface before and after contaminant exposure using a Thermo ESCALAB 250XI X-ray photoelectron system (Thermo Electron Corporation, USA).

Scanning electron microscope-Energy dispersive spectrometer (SEM-EDS) was used to examine changes in the morphology, structure, element species of Fe NPs before and after exposure to Pb(II) and rifampicin using a S4800 scanning electron microscope (Hitachi, Japan).

Transmission Electron Microscopy (TEM) images of Fe NPs were produced using a Tecnai G2 F20 instrument (FEI Corporation, USA) using a 200 kV accelerating voltage.

Specific surface area and the corresponding pore size of Fe NPs were determined using the Brunauer-Emmett-Teller (BET) method via a nitrogen adsorption-desorption techniques (BELSORP-mini II BEL Japan).

2.5. Batch experiments

Batch experiments were performed to analyze the effects of different experimental conditions on the removal efficiency of Pb(II) and rifampicin removal by Fe NPs.

A mixed aqueous solution of Pb(II) and rifampicin (25 mL) was added to 50 mL glass tubes which were placed on a 250 constant temperature shaker operating at 250 rpm. Samples were taken at time intervals of 5, 10, 20, 30, 60, 90, 120 min and under different conditions (solution concentrations of mixed Pb(II) and rifampicin: 10, 30 and 50 mg L^{-1}, pH: 3–5, Fe NPs concentrations 0.1, 0.5, 1.0 g L^{-1}, and temperatures 20, 30, 40 °C). The removal efficiency of Pb(II) and rifampicin by Fe NPs was determined in triplicate. The residual concentration of both Pb(II) and rifampicin in the filtrate were measured, using an atomic absorption spectrophotometer (VARIAN AA240, USA) at 273.8 nm, and a UV Spectrophotometer (UV-9000 UV–Vis, Yuanxi Instrument Co., Ltd., Shanghai) at 474 nm, respectively.

2.6. Preparation of spiked water

A spiked wastewater solution sample was prepared by dissolving rifampicin (0.05 g) and lead nitrate (0.08 g) in wastewater (100 mL), and then diluting the entire solution in a 1 L volumetric flask to give final concentrations of 50 mg L^{-1} for both Pb(II) and rifampicin.

The removal efficiency of Fe NPs for both Pb(II) and rifampicin was estimated using equation (1):

$$R(\%) = \frac{C0 - Ct}{C0} \times 100\% \quad (1)$$

Where R (%) was the removal efficiency of either Pb(II) or rifampicin, and C_0 and C_t were respectively, the initial concentration of contaminants at time 0 min and the residual concentrations of contaminants remaining in solution at time t min.

3. Results and discussion

3.1. Characterization

3.1.1. XRD analysis

The crystalline structures of the as-prepared Fe NPs before and after reaction with Pb(II) and rifampicin were examined via determination of X-ray diffraction (XRD) patterns (Fig. 1). No unique sharp diffraction peaks were observed in the XRD pattern, indicating that the synthesized Fe NPs was essentially amorphous (Wang et al., 2014). XRD patterns of Fe NPs before (Fig. 1a) and after (Fig. 1b) reaction with Pb(II) and rifampicin, were essentially identically and only exhibited a broad diffraction peak at 22.6°, which corresponded to amorphous carbon, suggesting the organic molecules from the green tea extract had successfully combined with Fe NPs and coated the surface of the Fe NPs (Wang et al., 2014). Additionally, since there was no significant change in the XRD pattern of Fe NPs after reaction with Pb(II) and rifampicin, this suggested that the removal mechanism for both contaminants was dominated by an adsorption process, in agreement with many previous studies (Kumar et al., 2013; Njagi et al., 2010). The lack of any discernible signals ascribed to either Fe or Pb(II) in any XRD pattern, did not mean they were not present, since the excessive cover of green tea derived organic molecules on the surface of Fe NPs may have masked any such peaks (Luo et al., 2016).

3.1.2. SEM-EDS analysis

The surface morphologies of the manufactured Fe NPs before (Fig. 2a) and after (Fig. 2b) adsorption reaction with Pb(II) and rifampicin were examined by SEM (Fig. 2). Prior to exposure to contaminants the exterior of Fe NPs was relatively coarse and the nanoparticles themselves were uniformly distributed and present in the form of chains (Fig. 2a). The diameters ranged from 30 to 100 nm (Smuleac et al., 2011), and seemed to be encapsulated by biomolecules from the green tea extract, which demonstrated that Fe NPs had been successfully synthesized (Wang et al., 2014). Conversely, after exposure to contaminants Fe NPs exhibited a large amount of agglomeration and the morphology became coarser, which was attributed to Pb(II) and rifampicin being adsorbed to the surface of Fe NPs.

The changes in surface composition before (Fig. 2c) and after (Fig. 2d) reaction with Pb(II) and rifampicin, were further examined using SEM-EDS spectra. Prior to the reaction the composition of Fe NPs was C (38.3%), O (24.3%) and Fe (37.5%). While oxygen may normally be present in Fe NPs as indicative of an iron oxide coating the large amount of carbon is almost exclusively found in green synthesizes Fe NPs. Thus, the large C and O signals observed for Fe NPs here originated primarily from polyphenol groups and other C and O-containing biomolecules present in green tea extracts (Kuang et al., 2013). After reaction there were consistent decreases in the percentage concentrations of C (36.0%), O (22.9%) and Fe (26.0%) coincident with the appearance of significant a new element Pb (15.1%) consistent with adsorption of Pb(II) by Fe NPs.

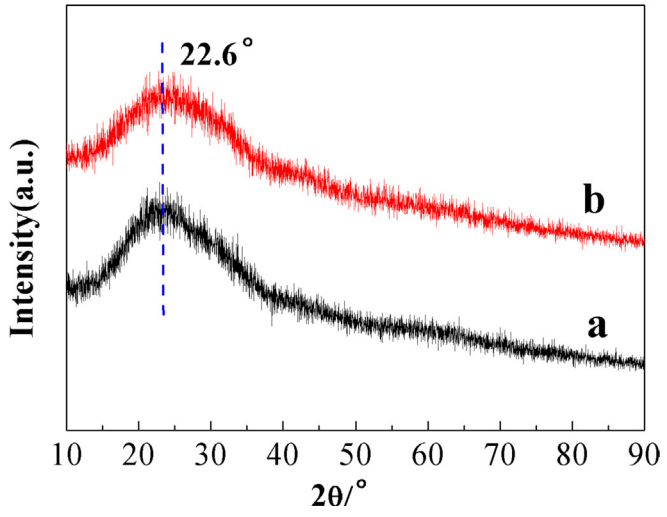

Fig. 1. XRD image of Fe NPs before (a) and after (b) reaction with Pb(II) and rifampicin.

3.1.3. TEM analysis

The TEM images of Fe NPs before and after adsorption of Pb(II) and rifampicin indicated that initially Fe NPs possessed a particle size between 30 and 100 nm and exhibited a generally dispersed appearance (Fig. 3a). However, after the reaction (Fig. 3b), while Fe NPs were more agglomerated, the size of individual particles hardly changed. Dark areas on the TEM image near the surface indicated that Pb and rifampicin were adsorbed on the Fe NPs (Rehman et al., 2019).

3.1.4. XPS

The composition and elemental distributions in a substances surface can also be studied using XPS analysis. In agreement with EDS the full scan XPS spectrum of the original Fe NPs indicated that it was composed exclusively of C, O, and Fe (Fig. 4a). The C1s spectra of Fe NPs (Fig. 4b) contained two signals which were attributed to hydroxyl groups (-C-OR) (285.8 eV) and aliphatic/aromatic carbon groups (CH_x, C—C/C═C) (284.4 eV) (Xie et al., 2019). This result was consistent with the results of both XRD and SEM-EDS analysis and indicated that Fe NPs was successfully synthesized via the green tea extract. The binding energy of Fe 2p (Fig. 4c) could be deconvoluted in to four components having energies of 706.0, 711.0, 719.9 and 725.3 eV, respectively, which were attributed to Fe^0, Fe $2p_{3/2}$ and Fe $2p_{1/2}$ species, respectively (Xie et al., 2019), it was confirmed that Fe_3O_4 mainly present in Fe NPs in two oxidation states of Fe^{2+} and Fe^{3+}, and there was a small amount of Fe^0 presented in Fe NPs (Wei et al., 2017). For Pb (Fig. 4d) two XPS peaks at 138.7 and 143.7 eV were clearly observed attributable to Pb 4f, demonstrating that Pb(II) was successfully adsorbed onto Fe NPs.

3.1.5. FTIR analysis

The functional groups present in rifampicin and Fe NPs before and after reaction with Pb(II) and rifampicin can be monitored by FTIR. Broad bands present at 3442 cm^{-1} (Fig. 5b and c) are attributable to stretching vibration of —OH due to the high moisture content of green tea plants (Huang et al., 2014; Wang et al., 2014). Characteristic peaks attributable to a range of rifampicin functional groups were distributed between 1723 cm^{-1} and 887 cm^{-1}. For example peaks at 1723, 1455 and 1247 cm^{-1} corresponded to —C═O, amide II and C—O—C vibrations, respectively (Das et al., 2010). Other peaks were attributable to -NH_3^{2+} (1644 cm^{-1}), C—OH (1447 cm^{-1}) and C—O (1046 cm^{-1}) function groups (Kumar et al., 2013), which corresponded to substances typically present in GT, such as tea polyphenols, catechols and amino acids, which proved that Fe NPs were successfully synthesized via GT acting as a reducing and capping agent (Pooja et al., 2015). Specifically the peak which appeared at 1455 cm^{-1}, was attributed to amide II, indicating that rifampicin was successfully adsorbed on to Fe NPs (Pooja et al., 2015).

3.1.6. BET analysis

The specific surface area, pore width and distribution of Fe NPs was measured via the N_2-BET adsorption method (Brunauere Emmette Teller isotherm). When the relative pressure rose to 0.8,

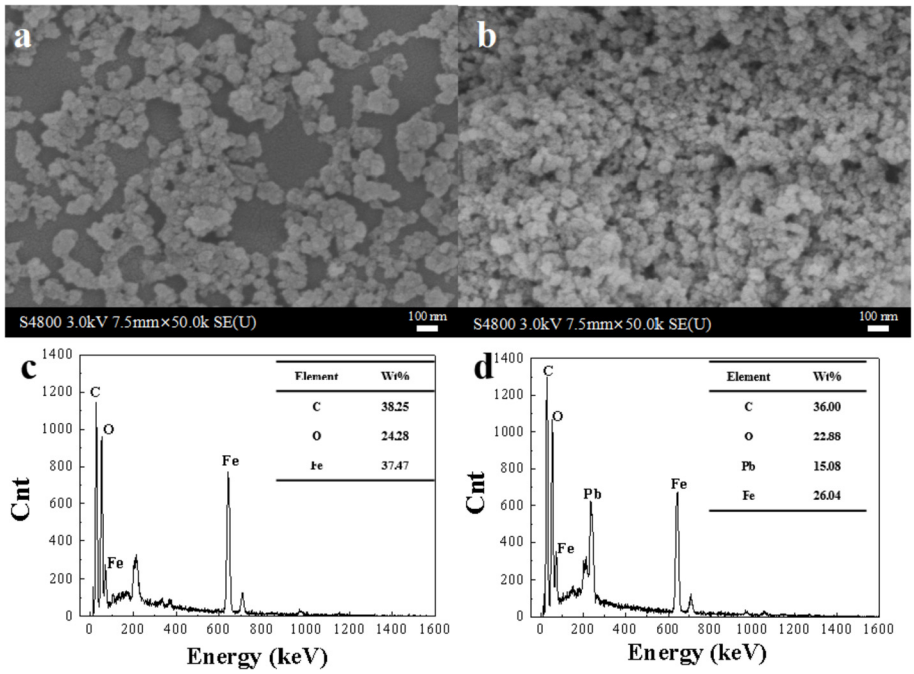

Fig. 2. SEM images for Fe NPs before (a) and after (b) Pb(II) and rifampicin adsorption; together with the corresponding EDS images for Fe NPs before (c) and after (d) Pb(II) and rifampicin adsorption.

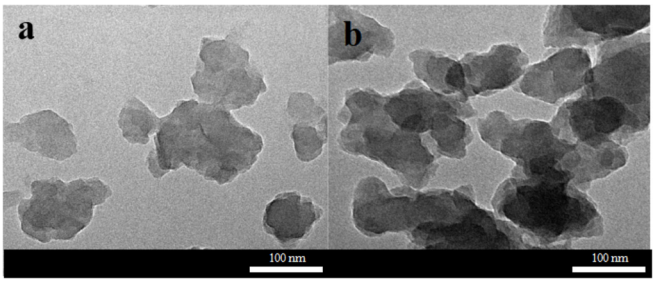

Fig. 3. TEM micrographs for Fe NPs before (a) and after (b) Pb(II) and rifampicin adsorption.

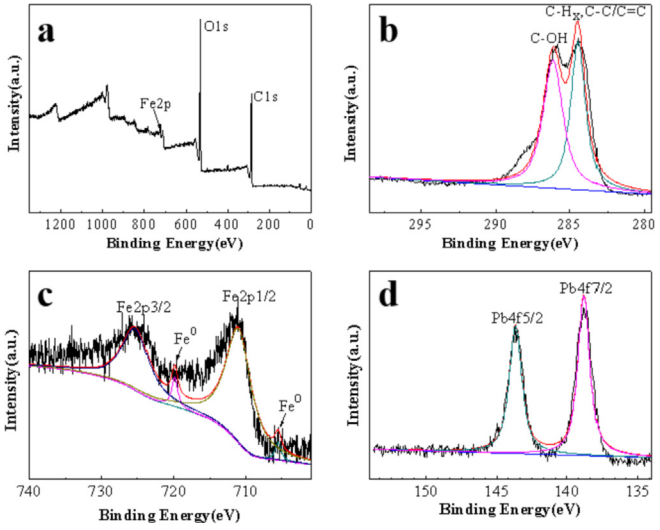

Fig. 4. Full XPS spectra of Fe NPs (a); C1s core level spectra of Fe NPs (b); Fe2p core level spectra of Fe NPs (c) and Pb4f core level spectra of Fe NPs after adsorption (d).

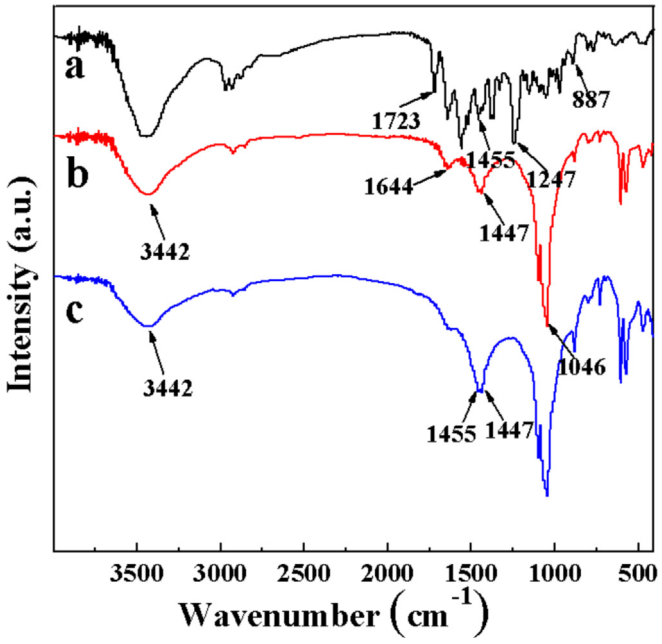

Fig. 5. FTIR spectra of rifampicin (a), Fe NPs (b) and Fe NPs after Pb(II) and rifampicin adsorption (c).

the adsorption amount was also significantly enhanced (Fig. 6a), indicating the presence of both mesopores and macropores in Fe NPs. Similarly, the pore size distribution diagram (Fig. 6b) showed that the pore width was mainly distributed between 30 and 100 nm, which further indicated that the structure of Fe NPs was mainly composed of meso-pores and macro-pores (Das et al., 2010). The specific surface area of Fe NPs was 37.3 $m^2 g^{-1}$, where the large specific surface area and the meso/macro-porous structures of Fe NPs offered numerous reaction sites for direct contact between the

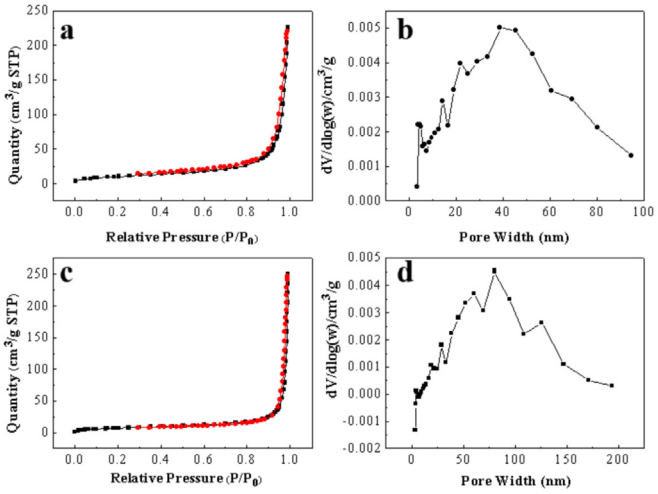

Fig. 6. Nitrogen adsorption-desorption isotherm and pore size distribution for Fe NPs (a, b) and nitrogen adsorption-desorption isotherm and pore size distribution for Fe NPs after Pb(II) and rifampicin adsorption (c, d).

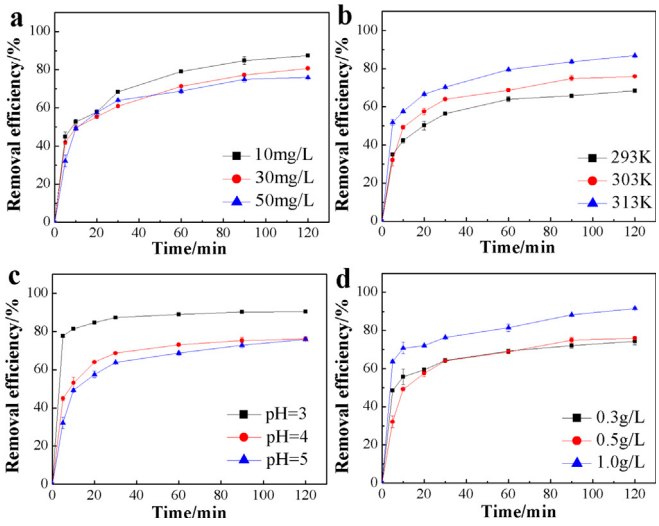

Fig. 8. Variation in the removal efficiency of rifampicin by Fe NPs with time under different experimental conditions.

adsorbent and the adsorbate (Sharma et al., 2019). However, the specific surface area of Fe NPs after adsorption decreased to 26.8 $m^2 g^{-1}$, which could be attributed to the closure of some pores in Fe NPs due to the adsorption of Pb(II) and rifampicin onto the Fe NPs surface (Naushad et al., 2016).

3.2. Removal of Pb(II) and rifampicin at different conditions

3.2.1. Effect of initial contaminant concentration

Changes in the initial concentration of contaminants in the range 10–50 mg L^{-1} did not dramatically change the adsorption of either Pb(II) (Fig. 7a) or rifampicin (Fig. 8a). As can be seen in Figs. 7a and 8a, for Pb (II), there was only a small decrease (<5%) in the removal efficiency at 50 mg L^{-1}, with no noticeable decreases at the lower two concentrations. For rifampicin the effect of initial concentration was more pronounced. However as with Pb(II), the removal efficiency of rifampicin also decreased with an increase in the initial rifampicin concentration. For both contaminants there were no significant differences in the removal efficiency when the initial contaminant concentrations were <30 mg L^{-1}, which indicated that at theses concentrations there were sufficient adsorption sites available for both Pb(II) and rifampicin. However, as the initial contaminant concentration increased the upper limit of the adsorption capacity of Fe NPs began to be exceeded, and consequently the residual solution concentrations of Pb(II) and

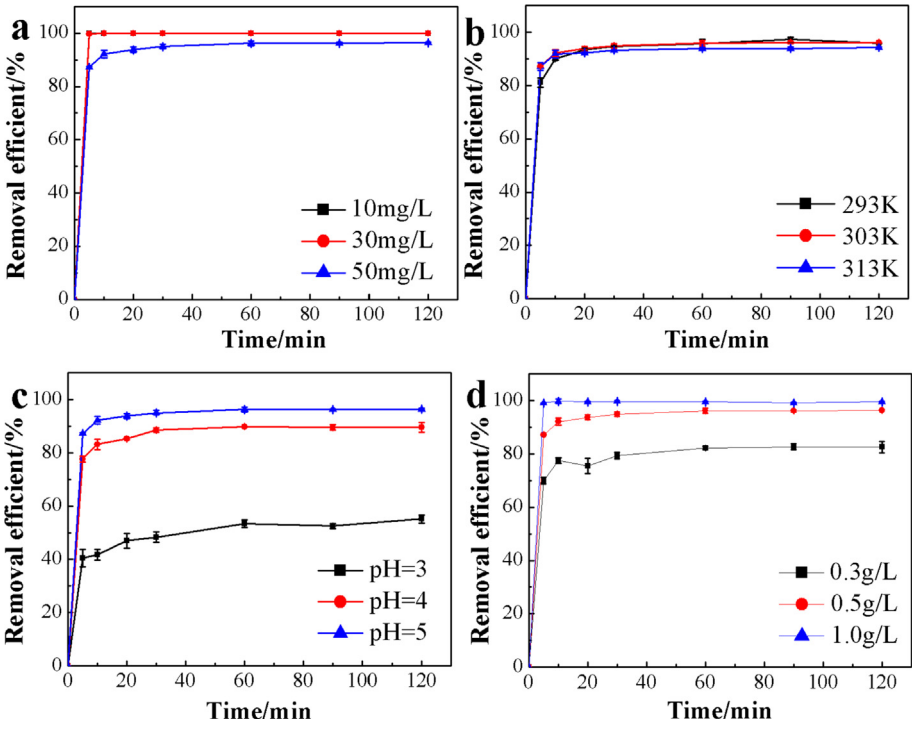

Fig. 7. Variation of removal efficiency of Pb(II) by Fe NPs with time under different experimental conditions.

rifampicin also increased (Cheera et al., 2016). These results confirmed that there was only a finite number of adsorption sites available for contaminant interaction on the Fe NPs and that when all of the adsorption sites were occupied, the removal efficiency decreased.

3.2.2. Effect of temperature

For Pb(II), changes in temperature in the range of 20–40 °C had minimal impact on the removal efficiency (Fig. 7b). The Pb removal efficiency was almost identical at 20 °C and 30 °C being 96.0% and 96.2%, respectively, and dropped to only 94.3% as the temperature was increased to 40 °C. However, in stark contrast, the removal efficiency of rifampicin increased with temperature (Fig. 8b), a phenomenon which was attributed to an increase in the Brownian movement, which enabled better contact between rifampicin molecules and Fe NPs leading to higher adsorption (Song et al., 2017).

3.2.3. Effect of pH

As pH was adjusted from 5 to 3 the Pb(II) removal efficiency also decreased from 96.4% to 55.2% (Fig. 7c). This suggested that at lower pH, the high concentration of H^+ in the solution allowed H^+ and Pb(II) to compete for a limited available adsorption sites on Fe NPs. However, in direct contrast the removal efficiency of rifampicin was significantly enhanced as pH decreased (Fig. 8c). This may be because as the pH increased, the positive charge on the rifampicin gradually decreased, thereby weakening the electrostatic attraction between rifampicin and Fe NPs, and reducing the removal efficiency (Cai et al., 2019).

3.2.4. Effect of dosage

As the dose of Fe NPs increased from 0.3 to 1 g L^{-1}, the removal efficiency of Pb(II) also increased from 82.6 to 99.6% (Fig. 7d) which signified that the number of available adsorption sites were greatly increased by an increased Fe NPs dose. Likewise the removal efficiency of rifampicin also increased from 74.3% to 91.6% as the Fe NPs dose increased (Fig. 8d). These results simply indicated that as Fe NP dose increased the number of active and adsorptive sites increased and the reactive surface area was more available, leading to an enhanced the removal efficiency (Wang et al., 2014).

3.3. Adsorption isotherms

The interaction between Fe NPs and both contaminants was further explored by studying adsorption isotherms. When the pH was unadjusted, batch experiments were carried out using contaminants with an initial concentration of 10–70 mg L^{-1}, and the data were fit to the Langmuir, Freundlich and Temkin adsorption isotherms. The Langmuir model assumes that the adsorption process is a single layer adsorption onto the adsorbent surface and is represented by equation (2):

$$\frac{Ce}{qe} = \frac{Ce}{qm} + \frac{1}{qmKL} \tag{2}$$

where q_e (mg·g^{-1}) is the amount of contaminants adsorbed at the time of equilibrium, C_e (mg·L^{-1}) is the concentration of residual contaminants in solution at equilibrium, q_m is the theoretical maximum adsorption capacity (mg·g^{-1}), and K_L (L·mg^{-1}) is the Langmuir constant.

The Freundlich isotherm assumes that energy-imbalanced adsorption sites exist on which multi-layer adsorption occurs and the adsorption isotherm model is described by equation (3):

$$lnqe = \ln KF + \frac{1}{n}\ln Ce \tag{3}$$

Where q_e (mg·g^{-1}) is the equilibrium adsorption capacity, C_e (mg·L^{-1}) is the concentration of contaminants in the solution at the equilibrium, K_F (mg·mg^{-1}) is the binding energy constant, which reflects the adsorption capacity of the adsorbate on contaminant, and n is the Freundlich constant, and the calculated data results were showed in Table 1Table 2).

The Temkin isothermal model assumes that an increase in adsorption capacity causes a linear decrease, rather than a logarithmic decrease, in adsorption heat (Sharma et al., 2018b) and is described by equation (4):

$$qe = B(ln\ Ce) + B(ln\ A) \tag{4}$$

Where B relevant to the heat of adsorption, and A (L·g^{-1}) is the binding constant of the maximum binding energy at adsorption equilibrium, C_e and q_e have the same meanings as above. Comparison of R^2 values for the three isotherm models considered here (Table 1) as a measure of goodness fit indicated that adsorptions of Pb(II) to Fe NPs was most consistent with the Langmuir model. The adsorption capacity at equilibrium was also close to the theoretical adsorption amount determined from the Langmuir model, indicating that the adsorption process of Pb(II) was mainly a spontaneous chemical adsorption process (Huang et al., 2018). As the temperature rose, K_L increased gradually, demonstrating that elevated temperatures slightly favored increased adsorption of Pb(II) by Fe NPs.

In contrast, it can be clearly seen from comparison of R^2 values (Table 1) that the Freundlich adsorption model was more consistent with the adsorption of rifampicin by Fe NPs suggesting that multilayer adsorption was involved As temperature increased from 293 to 303–313 K, n values decreased to 1.59, 1.21, 0.82, respectively; and K_F decreased to 12.90, 9.27, 5.61, respectively which was also consistent with the Freundlich adsorption model.

3.4. Adsorption kinetics

Adsorption kinetic data were fit to both the pseudo first-order and pseudo-second-order kinetic models expressed by equations (5) and (6) respectively.

The pseudo-first-order kinetic model:

$$\ln(qe - qt) = \ln qe - k1t \tag{5}$$

The pseudo-second-order kinetic model:

$$\frac{t}{qt} = \frac{1}{k2qe^2} + \frac{t}{qe} \tag{6}$$

Where, q_t and q_e were the adsorption amount (mg·g^{-1}) of either Pb(II) or rifampicin by Fe NPs at t time and at equilibrium, respectively and k_1 and k_2 were the pseudo-first-order and pseudo-second-order rate constants, respectively. The correlation coefficients (R^2) were used to measure the consistency of the experimental data to the respective kinetic models.

Irrespective of the reaction temperature, the kinetic data for both Pb(II) and rifampicin best fit the pseudo-second-order kinetic models (Table 1), with $R^2 > 0.999$. This indicated that the adsorption of both Pb(II) and rifampicin by Fe NPs most closely followed a pseudo-second order kinetic model where the adsorption mechanism of both contaminants by Fe NPs was via a chemisorption process (Zhang et al., 2018), which was consistent with the results of both the adsorption isotherm studies.

Table 1
Best fit isotherm parameters for Pb(II) and rifampicin adsorption on Fe NPs.

Temperature (K)/Contaminant	Freundlich			Langmuir			Temkin		
	n	K_F (mg·g^{-1})	R^2	q_m (mg·g^{-1})	K_L (L·mg^{-1})	R^2	A (L·g^{-1})	B	R^2
293/Pb(II)	3.12	30.82	0.884	80.00	0.74	0.995	0.07	44.64	0.963
303/Pb(II)	4.00	44.54	0.983	96.15	0.79	0.991	0.06	50.00	0.955
313/Pb(II)	4.10	50.96	0.982	100.00	1.45	0.987	0.06	52.63	0.949
293/Rif	1.59	7.74	0.917	92.59	0.06	0.944	0.09	34.13	0.961
303/Rif	1.21	5.56	0.930	188.68	0.03	0.687	0.08	38.61	0.946
313/Rif	0.82	3.36	0.981	204.08	0.02	0.640	0.07	50.51	0.922

Table 2
Best fit kinetic parameters for Pb(II) and rifampicin adsorption on Fe NPs.

Temperature(K)/Contaminant	Pseudo-first-order kinetic model			Pseudo-second-order kinetic model		
	k_1 (min^{-1})	q_{e1} (mg·g^{-1})	R^2	k_2 (g·mg^{-1}·min^{-1})	q_{e2} (mg·g^{-1})	R^2
293/Pb(II)	0.0247	2.263	0.915	0.0135	91.74	0.999
303/Pb(II)	0.0488	6.895	0.915	0.0194	93.46	1.000
313/Pb(II)	0.0430	3.319	0.982	0.0293	90.09	1.000
293/Rif	0.0318	30.73	0.964	0.0020	60.98	0.999
303/Rif	0.0320	38.19	0.973	0.0017	80.00	0.999
313/Rif	0.0261	27.45	0.992	0.0025	70.92	0.999

Table 3
Thermodynamic parameters for Pb(II) and rifampicin adsorption on Fe NPs.

Contaminant	ΔH_0 (kJ·mol^{-1})	ΔS_0 (kJ·mol^{-1})	ΔG_0 (kJ·mol^{-1})		
			293 K	303 K	313 K
Pb(II)	15.31	0.061	−2.58	−3.57	−3.79
rifampicin	23.08	0.081	−3.35	−4.62	−6.56

3.5. Adsorption thermodynamics

Adsorption thermodynamics of Pb(II) and rifampicin at an initial concentration of 50 mg L^{-1} by Fe NPs were quantified using batch studies under different temperatures, where the thermodynamic parameters were calculated using the following equations:

$$\ln\left(\frac{qe}{Ce}\right) = \frac{\Delta S_0}{R} - \frac{\Delta H_0}{RT} \quad (7)$$

$$\frac{qe}{Ce} = K \quad (8)$$

$$\Delta G_0 = -RT\ln K \quad (9)$$

Where, ΔS_o (kJ·mol^{-1}), ΔH_o (kJ·mol^{-1}) and ΔG_o (kJ·mol^{-1}) were the standard entropy change, enthalpy change and Gibbs free energy, respectively, calculated from the intercept and slope of a linear fit of ln q_e/C_e versus $1/T$. And thereafter the equilibrium coefficient K (L·mol^{-1}) was calculated from equation (8), where R was the universal gas constant (8.314 J mol·K^{-1}).

The derived thermodynamic parameters (Table 3), clearly indicate that for both contaminants the reaction was endothermic (Cai et al., 2019), with ΔH_0 values of 15.31 and 23.08 kJ mol^{-1} for Pb(II) and rifampicin, respectively, which was consistent with batch experiments conducted at different temperatures that had shown that contaminant adsorption efficiency increased with temperature. In addition, the negative value of ΔG_0 under different temperatures illustrated that the adsorption reaction was spontaneous.

In order to evaluate the potential practical effectiveness of the Fe NPs adsorbent developed here, the values of maximum adsorption capacity obtained here were compared with the values reported in the literature for a number of different adsorbents (Table 4). This comparison indicated that Fe NPs were indeed a promising material for removal of both Pb(II) and rifampicin from aqueous solution, with adsorption capacity far higher than most previously studied materials.

3.6. Removal mechanism of Pb(II) and rifampicin by Fe NPs

Based on the results described above, a possible mechanism for the simultaneous removal of Pb(II) and rifampicin by Fe NPs is illustrated in Fig. 9. It can be concluded that Fe NPs removes Pb(II) and rifampicin contaminants by the following two strategies 1) Pb(II) is adsorbed on to the surface of Fe NPs by virtue of the innate adsorption properties of iron oxides for metal ions, 2) Rifampicin and Pb(II) are both interact more specifically with the functional groups on the surface of Fe NPs.

3.7. Removal of Pb(II) and rifampicin from wastewater

To confirm whether Fe NPs could be practically employed to

Table 4
Comparison of adsorption capacities for selected heavy metal and organic pollutant removal using different adsorbents.

Adsorbent	Contaminant	Max adsorption capacity (mg·g^{-1})	Parameters	Reference
TIV	Pb(II), Hg(II)	18.8, 17.2	pH = 2–8, Temperature 20–50 °C	Naushad et al. (2015).
FSAC	Pb(II)	80.7	pH = 4, Temperature 60 °C	Ghasemi et al. (2014).
GA-cl-poly (AAm)	crystal violet	90.9	pH = 2–14, Temperature 35–75 °C	Sharma et al. (2018b).
GG-crosslinked-SL NHS	thiophanate methyl	59.2	pH = 1–10, Temperature 35–75 °C	Sharma et al. (2018a).
Fe NPs	Pb(II), rifampicin	100.0, 107.7	pH = 3–5, Temperature 20–40 °C	This work

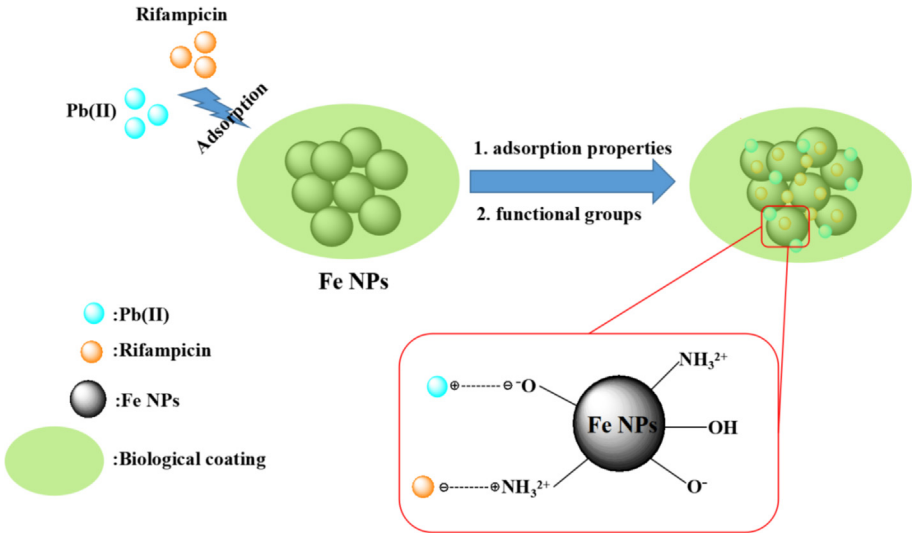

Fig. 9. Removal mechanism of Pb(II) and rifampicin by Fe NPs.

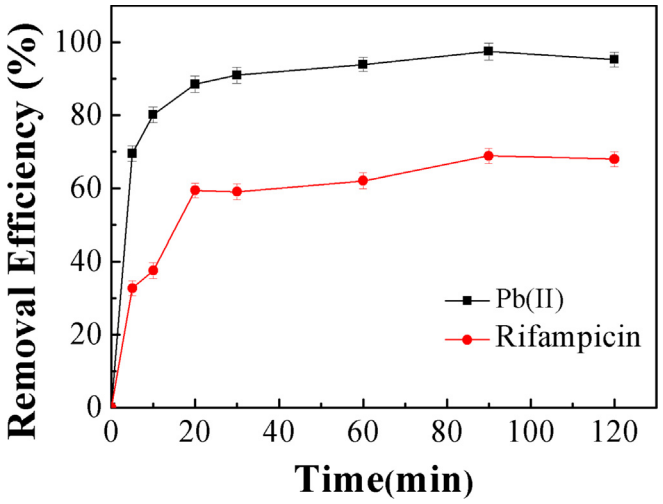

Fig. 10. The removal efficiency of Pb(II) and rifampicin by Fe NPs in a spiked wastewater sample. Conditions: dose: 0.5 g L^{-1}, temperature: 298 K, rotation speed: 250 rpm, pH = 5, initial Pb(II) and rifampicin concentrations: 50 mg L^{-1} each.

effectively simultaneously remove Pb(II) and rifampicin from an actual wastewater, a wastewater sample was collected from Fuzhou Wastewater Treatment Plant in China and treated with Fe NPs. As can be seen from Fig. 10, Fe NPs successfully removed 97.5% and 68.8% of Pb(II) and rifampicin, respectively quickly (<20 min) from the wastewater, which clearly indicated that Fe NPs had an excellent potential for the treatment of Pb(II) and rifampicin in wastewater.

3.8. Reusability

The reusability of an adsorbent is an important criterion when evaluating its practical utility. Here, the recyclability of the produced Fe NPs for Pb(II) adsorption was evaluated using three different regeneration solutions, 0.1 M HCl, absolute ethanol and deionized water. A 50 mg L^{-1} Pb(II) and rifampicin mixed solution (20 mL) was shaken with 10 mg Fe NPs at 250 rpm and 30 °C for 120 min. After 120 min, the supernatant liquid was centrifuged, filtered and analyze for residual concentrations of Pb(II) and rifampicin by AAS and UV–vis, before the remaining Fe NPs were washed several times by either 0.1M HCl, absolute ethanol or deionized water solution to remove the excess Pb(II) and rifampicin and thus regenerate the Fe NPs. After the washing an additional aliquot of 50 mg L^{-1} Pb(II) and rifampicin mixed solution (20 mL) was added and the removal and eluted again repeated using the steps as described above. The results (Fig. 11) showed relatively high removal efficiency of 52.3% and 64.9% for Pb(II) and rifampicin even after 5 cycles indicating that Fe NPs were highly reusable.

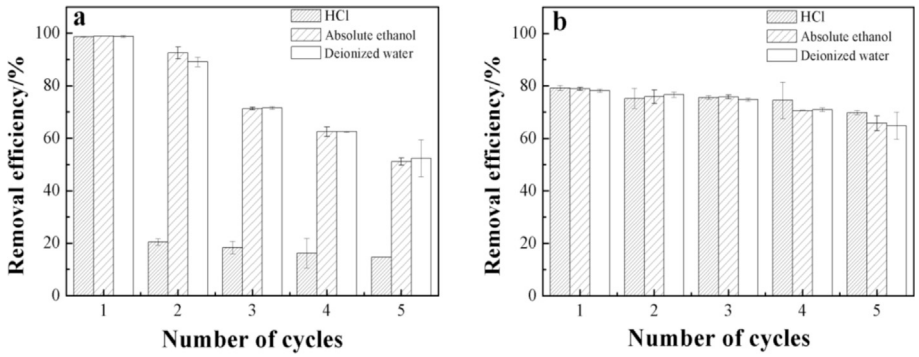

Fig. 11. Variation in removal efficiency (%) of Pb(II) (a) and rifampicin (b) by Fe NPs adsorption with number of reuse cycles.

4. Conclusions

In this paper green Fe NPs were initially fabricated by a facile, cheap and environment friendly synthetic method. The produced material was then shown to efficiently remove both Pb(II) and rifampicin from water; where removal efficiency of Pb(II) and rifampicin reached 97.5% and 68.8%, respectively, for a spiked wastewater sample. This indicated that this new material had proven potential as a cost effective and environmentally friendly adsorbent for the simultaneous treatment of Pb(II) and rifampicin from real wastewater. The adsorption of both Pb(II) and rifampicin by Fe NPs followed pseudo-second order kinetics, where the adsorption process was mainly via chemisorption. Overall, Fe NPs exhibited excellent environmental remediation performance, which was consider suitable for future applications in wastewater remediation.

Acknowledgements

The Fujian Province Innovation and Entrepreneurship Talents, China is gratefully acknowledged.

References

Bagbi, Y., Sarswat, A., Mohan, D., Pandey, A., Solanki, P.R., 2017. Lead and chromium adsorption from water using L-cysteine functionalized magnetite (Fe_3O_4) nanoparticles. Sci. Rep-UK. 7, 7672.

Cai, W.L., Weng, X.L., Chen, Z.L., 2019. Highly efficient removal of antibiotic rifampicin from aqueous solution using green synthesis of recyclable nano-Fe_3O_4. Environ. Pollut. 247, 839–846.

Calderon, B., Fullana, A., 2015. Heavy metal release due to aging effect during zero valent iron nanoparticles remediation. Water Res. 83, 1–9.

Cheera, P., Karlapudi, S., Sellola, G., Ponneri, V., 2016. A facile green synthesis of spherical Fe_3O_4 magnetic nanoparticles and their effect on degradation of methylene blue in aqueous solution. J. Mol. Liq. 221, 993–998.

Coll, M.T., Fortuny, A., Kedari, C.S., Sastre, A.M., 2012. Studies on the extraction of Co (II) and Ni (II) from aqueous chloride solutions using Primene JMT-Cyanex272 ionic liquid extractant. Hydrometallurgy 125, 24–28.

Das, R.K., Borthakur, B.B., Bora, U., 2010. Green synthesis of gold nanoparticles using ethanolic leaf extract of Centella asiatica. Mater. Lett. 64, 1445–1447.

Gao, J., Sun, S.P., Zhu, W.P., Chung, T.S., 2014. Chelating polymer modified P84 nanofiltration (NF) hollow fiber membranes for high efficient heavy metal removal. Water Res. 63, 252–261.

Ghasemi, M., Naushad, M., Ghasemi, N., Khosravi-fard, Y., 2014. A novel agricultural waste based adsorbent for the removal of Pb(II) from aqueous solution: kinetics, equilibrium and thermodynamic studies. J. Ind. Eng. Chem. 20, 454–461.

Guo, M.Y., Weng, X.L., Wang, T., Chen, Z.L., 2017. Biosynthesized iron-based nanoparticles used as a heterogeneous catalyst for the removal of 2, 4-dichlorophenol. Separ. Purif. Technol. 175, 222–228.

Huang, L.L., Weng, X.L., Chen, Z.L., Megharaj, M., Naidu, R., 2014. Synthesis of iron-based nanoparticles using oolong tea extract for the degradation of malachite green. Spectrochim. Acta A. 117, 801–804.

Huang, Q.Q., Chen, Y., Yu, H.Q., Yan, L.G., Zhang, J.H., Wang, B., Du, B., Xing, L.T., 2018. Magnetic graphene oxide/MgAl-layered double hydroxide nanocomposite: one-pot solvothermal synthesis, adsorption performance and mechanisms for Pb^{2+}, Cd^{2+}, and Cu^{2+}. Chem. Eng. J. 341, 1–9.

Hudcová, B., Veselska, V., Filip, J., Číhalová, S., Komárek, M., 2018. Highly effective Zn (II) and Pb (II) removal from aqueous solutions using Mg-Fe layered double hydroxides: comprehensive adsorption modeling coupled with solid state analyses. J. Clean. Prod. 171, 944–953.

Ioannou-Ttofa, L., Raj, S., Prakash, H., Fatta-Kassinos, D., 2019. Solar photo-Fenton oxidation for the removal of ampicillin, total cultivable and resistant E. coli and ecotoxicity from secondary-treated wastewater effluents. Chem. Eng. J. 355, 91–102.

Kuang, Y., Wang, Q.P., Chen, Z.L., 2013. Heterogeneous Fenton-like oxidation of monochlorobenzene using green synthesis of iron nanoparticles. J. Colloid Interface Sci. 140, 67–73.

Kumar, K.M., Mandal, B.K., Kumar, K.S., Reddy, P.S., Sreedhar, B., 2013. Biobased green method to synthesise palladium and iron nanoparticles using Terminalia chebula aqueous extract. Spectrochim. Acta A. 102, 128–133.

Li, Z., Wang, L., Meng, J., Liu, X., Xu, J., Wang, F., Brookes, P., 2018. Zeolite-supported nanoscale zero-valent iron: new findings on simultaneous adsorption of Cd (II), Pb (II), and as (III) in aqueous solution and soil. J. Hazard Mater. 344, 1–11.

Luo, F., Yang, D., Chen, Z.L., Megharaj, M., Naidu, R., 2016. One-step green synthesis of bimetallic Fe/Pd nanoparticles used to degrade Orange II. J. Hazard Mater. 303, 145–153.

Mahto, A., Kumar, A., Chaudhary, J.P., Bhatt, M., Sharma, A.K., Paul, P., Nataraj, S.K., Meena, R., 2018. Solvent-free production of nano-FeS anchored graphene from Ulva fasciata: a scalable synthesis of super-adsorbent for lead, chromium and dyes. J. Hazard Mater. 353, 190–203.

Naushad, M., 2014. Surfactant assisted nano-composite cation exchanger: development, characterization and applications for the removal of toxic Pb^{2+} from aqueous medium. Chem. Eng. J. 235, 100–108.

Naushad, M., ALOthman, Z.A., Awual, M.R., Alam, M.M., Eldesoky, G.E., 2015. Adsorption kinetics, isotherms, and thermodynamic studies for the adsorption of Pb^{2+} and Hg^{2+} metal ions from aqueous medium using Ti (IV) iodovanadate cation exchanger. Ionics 21, 2237–2245.

Naushad, M., Ahamad, T., Sharma, G., Al-Muhtaseb, A.H., Albadarin, A.B., Alam, M.M., ALOthman, Z.A., Alshehri, S.M., Ghfar, A.A., 2016. Synthesis and characterization of a new starch/SnO_2 nanocomposite for efficient adsorption of toxic Hg^{2+} metal ion. Chem. Eng. J. 300, 306–316.

Njagi, E.C., Huang, H., Stafford, L., Genuino, H., Galindo, H.M., Collins, J.B., Hoag, G.E., Suib, S.L., 2010. Biosynthesis of iron and silver nanoparticles at room temperature using aqueous sorghum bran extracts. Langmuir 27, 264–271.

Peiris, C., Gunatilake, S.R., Mlsna, T.E., Mohan, D., Vithanage, M., 2017. Biochar based removal of antibiotic sulfonamides and tetracyclines in aquatic environments: a critical review. Bioresour. Technol. 246, 150–159.

Pooja, D., Tunki, L., Kulhari, H., Reddy, B.B., Sistla, R., 2015. Characterization, bio-recognitive activity and stability of WGA grafted lipid nanostructures for the controlled delivery of Rifampicin. Chem. Phys. Lipids 193, 11–17.

Rehman, M., Rehman, W., Waseem, M., Hussain, S., Haq, S., Rehman, M.A., 2019. Adsorption mechanism of Pb^{2+} ions by Fe_3O_4, SnO_2, and TiO_2 nanoparticles. Environ. Sci. Pollut. Res. 26, 19968–19981.

Sharma, G., Kumar, A., Devi, K., Sharma, S., Naushad, M., Ghfar, A.A., Ahamad, T., Stadler, F.J., 2018a. Guar gum-crosslinked-Soya lecithin nanohydrogel sheets as effective adsorbent for the removal of thiophanate methyl fungicide. Int. J. Biol. Macromol. 114, 295–305.

Sharma, G., Kumar, A., Naushad, M., García-Peñas, A., Al-Muhtaseb, A.H., Ghfar, A.A., Sharma, V., Ahamad, T., Stadler, F.J., 2018b. Fabrication and characterization of Gum Arabic-cl-poly (acrylamide) nanohydrogel for effective adsorption of crystal violet dye. Carbohydr. Polym. 202, 444–453.

Sharma, G., Bhogal, S., Gupta, V.K., Agarwal, S., Kumar, A., Pathania, A., Mola, G.T., Stadler, F.J., 2019. Algal biochar reinforced trimetallic nanocomposite as adsorptional/photocatalyst for remediation of malachite green from aqueous medium. J. Mol. Liq. 275, 499–509.

Smuleac, V., Varma, R., Sikdar, S., Bhattacharyya, D., 2011. Green synthesis of Fe and Fe/Pd bimetallic nanoparticles in membranes for reductive degradation of chlorinated organics. J. Membr. Sci. 379, 131–137.

Song, X.L., Li, L., Geng, Z.R., Zhou, L., Ji, L.J., 2017. Effective and selective adsorption of As(III) via imprinted magnetic Fe_3O_4/HTCC composite nanoparticles. J. Environ. Chem. Eng. 5, 16–25.

Wang, T., Lin, J.J., Chen, Z.L., Megharaj, M., Naidu, R., 2014. Green synthesized iron nanoparticles by green tea and eucalyptus leaves extracts used for removal of nitrate in aqueous solution. J. Clean. Prod. 83, 413–419.

Wei, Y.F., Fang, Z.Q., Zheng, L.C., Tsang, E.P., 2017. Biosynthesized iron nanoparticles in aqueous extracts of Eichhornia crassipes and its mechanism in the hexavalent chromium removal. Appl. Surf. Sci. 399, 322–329.

Weng, X.L., Lin, S., Zhong, Y.H., Chen, Z.L., 2013. Chitosan stabilized bimetallic Fe/Ni nanoparticles used to remove mixed contaminants-amoxicillin and Cd (II) from aqueous solutions. Chem. Eng. J. 229, 27–34.

Xie, Y.Y., Yuan, X.Z., Wu, Z.B., Zeng, G.M., Jiang, L.B., Peng, X., Li, H., 2019. Adsorption behavior and mechanism of Mg/Fe layered double hydroxide with Fe_3O_4-carbon spheres on the removal of Pb(II) and Cu(II). J. Colloid Interface Sci. 536, 440–455.

Yan, W., Herzing, A.A., Kiely, C.J., Zhang, W.X., 2010. Nanoscale zero-valent iron (nZVI): aspects of the core-shell structure and reactions with inorganic species in water. J. Contam. Hydrol. 118, 96–104.

Zhang, K.X., Li, H.Y., Xu, X.J., Yu, H.W., 2018. Synthesis of reduced graphene oxide/NiO nanocomposites for the removal of Cr (VI) from aqueous water by adsorption. Microporous Mesoporous Mater. 255, 7–14.

Zhao, S., Ba, C., Yao, Y., Zheng, W., Economy, J., Wang, P., 2018. Removal of antibiotics using polyethylenimine cross-linked nanofiltration membranes: relating membrane performance to surface charge characteristics. Chem. Eng. J. 335, 101–109.